# Stable Bromonium and Iodonium Ions of the Hindered Olefins Adamantylideneadamantane and Bicyclo[3.3.1]nonylidenebicyclo[3.3.1]nonane. X-Ray Structure, Transfer of Positive Halogens to Acceptor Olefins, and *ab Initio* Studies

**R. S. Brown,*,† R. W. Nagorski,† A. J. Bennet,†,‡ R. E. D. McClung,*,† G. H. M. Aarts,† M. Klobukowski,*,† R. McDonald,§ and B. D. Santarsiero§,∥**

*Contribution from the Department of Chemistry and Structure Determination Laboratory, University of Alberta, Edmonton, Alberta, Canada, T6G 2G2*

*Received October 21, 1993®*

**Abstract:** The cyclic three-membered bromonium and iodonium ions of adamantylideneadamantane (Ad=Ad; **1**) have been prepared and characterized as their triflate salts (**1**-$Br^+$/$OTf^-$; **1**-$I^+$/$OTf^-$) by X-ray diffraction. The X-ray diffraction data indicate that the halonium ion portions of **1**-$Br^+$/$OTf^-$ and **1**-$I^+$/$OTf^-$ are essentially symmetrical with the following averaged structural parameters: Br–C, 2.11 Å; C–C, 1.49 Å; Br–C–C angle, 69.4°; C–Br–C angle, 41.3°; I–C, 2.48 Å; C–C, 1.45 Å; I–C–C angle, 72°; C–I–C angle, 36°. The $^{13}C$ NMR spectra of these ions and the bromonium and iodonium ions of bicyclo[3.3.1]nonylidenebicyclo[3.3.1]nonane (**2**) have been investigated in $CH_2Cl_2$. At low temperatures, the $^{13}C$ NMR spectra of **1**-$X^+$ (X = Br, I) and **2**-$I^+$ indicate that the halonium ion has two perpendicular planes of symmetry. Addition of the parent olefin causes line broadening of certain signals attributable to the carbon atoms above and below a plane that includes the central C–C bond and is perpendicular to the above two planes. The broadening suggests that small amounts of parent olefin can translocate the $X^+$ from the top side of a given halonium ion to its bottom side. Line-shape analysis yields the pseudo-first-order rate constant for site exchange at each concentration of added parent olefin. For **1**-$Br^+$, **1**-$I^+$, and **2**-$I^+$, the respective second-order rate constants for this site exchange are 2.0, 7.6, and 4.2 × $10^6$ $M^{-1}$ $s^{-1}$ at −80 °C. The activation parameters for the site exchange between **1**-$Br^+$ and Ad=Ad are $\Delta H^\ddagger$ = 1.8 kcal/mol and $\Delta S^\ddagger$ = −21 eu. High-level *ab initio* calculations on the model system $C_2H_4X^+ + C_2H_4 \rightleftharpoons C_2H_4 + C_2H_4X^+$ indicate that the transfer proceeds via an unsymmetrical 1:1 halonium ion/olefin charge-transfer complex intermediate and a symmetrical $D_{2d}$ transition state.

## Introduction

Ever since Strating, Wieringa, and Wynberg reported[1] that $Br_2$ reacts with adamantylideneadamantane (Ad=Ad; **1**) to produce a yellow, solid bromonium ion–tribromide salt, that system has attracted interest as the only known stable three-membered bromonium ion[2] (**1**-$Br^+$/$Br_3^-$). In non-nucleophilic solvents such as halogenated hydrocarbons, an equilibrium between **1**-$Br^+$/$Br_3^-$, Ad=Ad, the Ad=Ad:$Br_2$ charge-transfer complex (CTC), and what is believed to be **1**-$Br^+$/$Br_5^-$ is instantly established.[2c] This equilibrium complicates the analysis of the solution properties of any of the components of eq 1.[2c,e] Recently, we have reported[2d] that the $Br_3^-$ counterion can be replaced by the nearly non-nucleophilic triflate counterion ($CF_3SO_3^-$; $OTf^-$) simply by treating **1**-$Br_3^-$ or a mixture of one part Ad=Ad and two or more parts $Br_2$ with excess $CH_3SO_3CF_3$. Removal of the

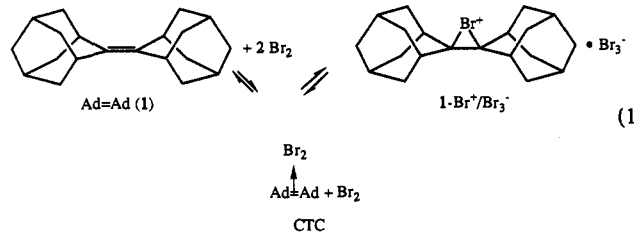


(1)

volatile products ($CH_3Br$, residual $Br_2$, and $CH_3SO_3CF_3$) affords a white solid (**1**-$Br^+$/$OTf^-$) that is sufficiently stable for a variety of purposes.

The most unusual property of **1**-$Br^+$/$OTf^-$ proves to be its propensity to undergo a remarkably fast degenerate transfer of $Br^+$ to free olefin (eq 2). Since the transfer must proceed via a

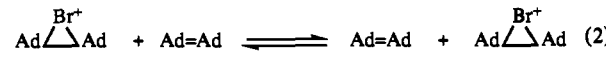


(2)

transition state where the $Br^+$ is coordinated to two Ad=Ad units, this unprecedented process might be a general phenomenon for halonium ions that are structurally prevented from undergoing any of the usual product-forming steps. Herein we report that the corresponding iodonium ions of Ad=Ad (**1**-$I^+$/$OTf^-$) and bicyclo[3.3.1]nonylidenebicyclo[3.3.1]nonane (**2**-$I^+$/$OTf^-$) also undergo this degenerate $X^+$ transfer to the corresponding free olefins. In addition, we report the crystal structures of **1**-$Br^+$/$OTf^-$ and **1**-$I^+$/$OTf^-$ determined by X-ray diffraction. Finally, we report a detailed *ab initio* theoretical description of the bonding in the model halonium ion $C_2H_4X^+$ and an analysis for the

† Department of Chemistry.
‡ Present address: Department of Chemistry, Simon Fraser University, Burnaby, BC, V5A 1S6.
§ Structure Determination Laboratory, Department of Chemistry.
∥ Present address: Molecular Structure Corporation, 3200A Research Forest Drive, The Woodlands, TX 77381-4238.
® Abstract published in *Advance ACS Abstracts*, February 1, 1994.

(1) Strating, J.; Wieringa, J. H.; Wynberg, H. *J. Chem. Soc., Chem. Commun.* **1969**, 907.
(2) (a) Olah, G. A.; Schilling, P.; Westerman, P. W.; Lin, H. C. *J. Am. Chem. Soc.* **1974**, *96*, 3581. (b) Slebocka-Tilk, H.; Ball, R. G.; Brown, R. S. *Ibid.* **1985**, *107*, 4504. (c) Bellucci, G.; Bianchini, R.; Chiappe, C.; Marioni, F.; Ambrosetti, R.; Brown, R. S.; Slebocka-Tilk, H. *Ibid.* **1989**, *111*, 2640. (d) Bennet, A. J.; Brown, R. S.; McClung, R. E. D.; Klobukowski, M.; Aarts, G. H. M.; Santarsiero, B. D.; Bellucci, G.; Bianchini, R. *Ibid.* **1991**, *103*, 8532. (e) Bellucci, G.; Bianchini, R.; Chiappe, C.; Ambrosetti, R.; Catalano, D.; Bennet, A. J.; Slebocka-Tilk, H.; Brown, R. S. *J. Org. Chem.* **1993**, *58*, 3401.

0002-7863/94/1516-2448$04.50/0 © 1994 American Chemical Society

**Table 1.** $^{13}C$ NMR Chemical Shifts for Various Halonium Ions and Parent Olefins[a]

| | assignments and chemical shifts (ppm) | | | | | | |
|---|---|---|---|---|---|---|---|
| olefin | 2,2′ | 1,1′,-3,3′ | 8,8′,-10,10′ | 4,4′,-9,9′ | 7,7′ | 5,5′ | 6,6′ |
| 1[b] | 133.66 | 32.44 | 40.01 | 40.01 | 39.16 | 39.16 | 37.76 |
| 1-Br$^+$/OTf$^-$ [c,d] | 156.24 | 36.99 | 42.69 | 40.31 | 26.57 | 26.54 | 36.18 |
| 1-Br$^+$/Br$_3^-$ [e] | 158.6 | 39.8 | 45.0 | 42.9 | 29.3 | 29.3 | 38.8 |
| 1-I$^+$/OTf$^-$ [c,d] | 149.57 | 36.74 | 42.88 | 41.88 | 26.67 | 26.55 | 36.59 |
| 1-I$^+$/OTf$^-$ [c,f] | 148.37 | 36.67 | 42.02 | 42.02 | 26.64 | 26.64 | 36.56 |
| 1-I$^+$/BF$_4^-$ [c,f] | 151.52 | 37.90 | 43.33 | 43.33 | 27.63 | 27.63 | 37.46 |
| 1-I$^+$/CN$^-$ [g] | 153.6 | 38.4 | 42.3 | 38.7 | 26.5 | 26.5 | 35.7 |
| 2[b] | 132.68 | 32.44 | 34.31 | 34.31 | 22.70 | 22.70 | |
| 2-Br$^+$/OTf$^-$ [c,d] | 159.33 | 37.23 | 38.33 | 36.37 | 20.63 | 20.63 | |
| 2-I$^+$/OTf$^-$ [c,d] | 151.40 | 36.63 | 38.45 | 36.74 | 20.06 | 19.93 | |
| 2-I$^+$/OTf$^-$ [c,f] | 150.91 | 36.26 | 37.23 | 37.23 | 19.73 | 19.73 | |

[a] In $CD_2Cl_2$ unless otherwise specified. [b] Ambient temperature. [c] −80 ± 2 °C. [d] Slow exchange limit; no added parent olefin. [e] In $Br_2$ solvent; ref 2a. [f] Fast exchange limit; with added parent olefin. [g] $SO_2$ solvent, −70 °C, slow exchange limit; ref 2a.

degenerate halonium ion transfer using the model reaction $C_2H_4X^+ + C_2H_4 \rightleftharpoons C_2H_4 + C_2H_4X^+$.

1-I$^+$/OTf$^-$ 2-I$^+$/OTf$^-$

## Experimental Section

**(a) General.** Routine NMR and IR spectra were recorded using Bruker WP-200 and Nicolet 5 × 20 FTIR spectrometers, respectively. All low-temperature $^{13}C$ NMR spectra were recorded using a Bruker WH-400 spectrometer. The NMR probe temperatures were measured using a calibrated Sensotek BAT-10 external thermocouple inserted directly into the probe and equilibrated for 15 min.

**(b) Materials.** Adamantylideneadamantane (**1**) was prepared as previously described.[3] Bicyclo[3.3.1]nonan-9-one was prepared[4] and coupled to form bicyclo[3.3.1]nonylidenebicyclo[3.3.1]nonane (**2**) by a procedure analogous to that reported.[5] It was finally purified by sublimation (gentle warming, 2 Torr) to provide a 30% overall yield: mp 143–144 °C; lit.[5] 144–146 °C. The $^1H$ NMR spectrum agreed with that reported.[5]

The bromonium triflate of **1** (**1**-Br$^+$/OTf$^-$) was synthesized as previously described.[2d] The corresponding iodonium triflate (**1**-I$^+$/OTf$^-$) was synthesized by the addition of a saturated solution of $I_2$ in purified[6a] $CH_2Cl_2$ to a $CH_2Cl_2$ solution containing equimolar amounts of **1** (0.1–0.25 g in 15–25 mL) and AgOTf cooled to 0 °C. The $I_2$ was added until a pink color persisted. The mixture was filtered through a Pasteur pipet containing a plug of glass wool to remove the solid AgI. The iodonium salt (**1**-I$^+$/OTf$^-$) is soluble in $CH_2Cl_2$ but can be precipitated by the addition of 120–190 mL of purified[6b] hexanes and cooling to −20 °C. The organic layer was decanted from the solid, which was then dried at −15 to 25 °C under high vacuum. $^{13}C$ NMR parameters for **1**-I$^+$/OTf$^-$ and **1**-Br$^+$/OTf$^-$ are given in Table 1.

The bromonium and iodonium triflates of olefin **2** were synthesized in an analogous fashion, but, for **2**-Br$^+$/OTf$^-$, the temperature had to be maintained at −60 to −80 °C to prevent decomposition. Their $^{13}C$ NMR parameters are also given in Table 1.

**(c) X-ray Diffraction.** Crystals of **1**-Br$^+$/OTf$^-$ were prepared from a solution of 319.7 mg of **1** (1.19 mmol) in 25 mL of dry $CH_2Cl_2$ containing $Br_2$ (0.25 mL, 4.85 mmol) and $CH_3SO_3CF_3$ (1 mL, 8.84 mmol) that was stirred for 1 h under Ar with protection from light. Evaporation of the volatiles yielded a crude yellow crystalline residue, which was treated for 1 h with 15 mL of $CH_2Cl_2$ containing 0.5 mL of $CH_3SO_3CF_3$. The volatiles were again evaporated to yield a pale yellow residue that was dissolved in 20 mL of $CH_2Cl_2$, and to this was added 60 mL of hexanes, which induced precipitation. The mother liquors were removed by syringe, and the process was repeated. The residue was treated with 10 mL of $CH_2Cl_2$ and filtered under Ar. The residue was washed with 10 mL of $CH_2Cl_2$, and the combined portions were treated carefully with 20 mL of hexane to induce turbidity. The mixture was then placed in a refrigerator, followed by placement in a −30 °C freezer to obtain white crystals suitable for X-ray diffraction.

Crystals of the iodonium salt (**1**-I$^+$/OTf$^-$) were prepared by placing a $CH_2Cl_2$ solution of crude **1**-I$^+$/OTf$^-$ ($10^{-3}$-$10^{-2}$ M) containing a slight excess of $I_2$ into the lower chamber of a Pasteur pipet that was sealed at the bottom and constricted in the center. Into the upper chamber was placed dry hexane. The tube was capped with a septum and stored at −15 to −20 °C until crystals of suitable size had appeared at the constriction. In Tables 1S and 2S (supplementary material) are complete listings of the diffraction data for **1**-Br$^+$/OTf$^-$ and **1**-I$^+$/OTf$^-$.

**(d) Dynamic $^{13}C$ NMR. (i) 1-Br$^+$/OTf$^-$.** Two 0.5-cm-diameter NMR tubes with Teflon inserts were charged with ~0.5 mL of a 100 mM solution of **1**-Br$^+$/OTf$^-$ in purified[6a] $CD_2Cl_2$. The stoppered tubes were then cooled immediately and stored at −78 °C in a dry ice bath until required. The first tube was inserted into the NMR probe, which had been equilibrated at −81 °C (thermocouple), and after 15 min, the $^{13}C$ NMR spectrum was collected. In a repetitive manner, the tube was removed and opened and to it was added a 10-μL aliquot of a 17.88 mM solution of Ad=Ad in $CD_2Cl_2$. After each addition, the tube was reinserted into the NMR probe and equilibrated at −81 °C for 15 min, and the $^{13}C$ spectrum was collected. When the spectral line shape indicated that the fast exchange limit had been reached, the experiment was repeated with the second tube. The rate constants for the site exchange were evaluated by line-shape analysis of the two carbon signals corresponding to $C_{8,8',10,10'}$ and $C_{4,4',9,9'}$ (see eq 3 below for assignments).

**(ii) Activation Parameters for Site Exchange with 1-Br$^+$/OTf$^-$.** A 0.5-cm NMR tube with a Teflon insert was charged with ~0.5 mL of a 100 mM solution of **1**-Br$^+$/OTf$^-$ in $CD_2Cl_2$ and inserted into the NMR probe at −80 °C. In the same manner as described above, aliquots of a 17.88 mM solution of **1** in $CD_2Cl_2$ were added until the signals corresponding to $C_{8,8',10,10'}$ and $C_{4,4',9,9'}$ showed sizeable exchange broadening. At that point, the temperature of the NMR probe was varied from −103.1 to −53.1 °C (six temperatures, measured by external thermocouple, equilibrated for 30 min) and the $^{13}C$ NMR spectrum collected at each temperature. Site exchange rate constants were evaluated by line-shape analysis.

**(iii) Site Exchange of I$^+$ between Iodonium Ions and Parent Olefins.** The rates of chemical exchange of I$^+$ between **1**-I$^+$/OTf$^-$ and olefin **1**, and between **2**-I$^+$/OTf$^-$ and olefin **2**, were evaluated using procedures similar to that described above. However, even after careful purification, the solutions of **1**-I$^+$/OTf$^-$ and **2**-I$^+$/OTf$^-$ contained residual olefin so that the peaks for $C_{8,8',10,10'}$ and $C_{4,4',9,9'}$ were coalesced in the $^{13}C$ NMR spectra at −80 °C. The residual olefin **1** in the solution of **1**-I$^+$/OTf$^-$ was protonated by addition of small aliquots of HOTf so that it did not participate in the exchange reaction. This procedure did not remove residual **2** from the solution of **2**-I$^+$/OTf$^-$, so the solution was filtered through a Pasteur pipet plugged with glass wool impregnated with 5–15 mg of solid AgOTf to complex the residual **2** and prevent its participation in the exchange process. Solutions of **1**-I$^+$/OTf$^-$ and of **2**-I$^+$/OTf$^-$ in $CD_2Cl_2$ were treated as described above and then maintained at −80 °C in the NMR probe between successive additions of small aliquots of 0.69 mM (**1**) or 21 mM (**2**) solutions of the respective olefins in $CD_2Cl_2$. The rate constants for the iodonium ion–olefin exchange reactions were determined by analysis of the $^{13}C$ NMR line shapes of the $C_{8,8',10,10'}$ and $C_{4,4',9,9'}$ resonances.

The observed variations in the rates of the halonium ion–olefin exchange reactions with [added olefin] are given in Table 3S (supplementary material) for the three systems studied.

## Results and Discussion

**(a) Structures of 1-Br$^+$/OTf$^-$ and 1-I$^+$/OTf$^-$.** Shown in Figures 1a,b and 2a,b are two views of each of the structures of **1**-Br$^+$/OTf$^-$ and **1**-I$^+$/OTf$^-$ as determined by X-ray diffraction. For **1**-Br$^+$/OTf$^-$, there are two independent bromonium ions in the asymmetric unit. Separating these is a region containing three triflate anions, one $H_3O^+$, and a $CH_2Cl_2$ of crystallization. This is best visualized from the representation given in Figure 1b viewed along an axis drawn between the two bromines. Nonbonded

(3) Fleming, M. P.; McMurray, J. E. *Org. Synth.* **1981**, *60*, 113.
(4) Foote, C. S.; Woodward, R. B. *Tetrahedron* **1964**, *20*, 687.
(5) Keul, H. *Chem. Ber.* **1975**, 108, 1207.
(6) (a) Perrin, D. D.; Armarego, W. L. F.; Perrin, D. R. *Purification of Laboratory Chemicals*, 2nd ed.; Pergamon Press: Toronto, 1981; p 205. (b) *Ibid.*, p 283.

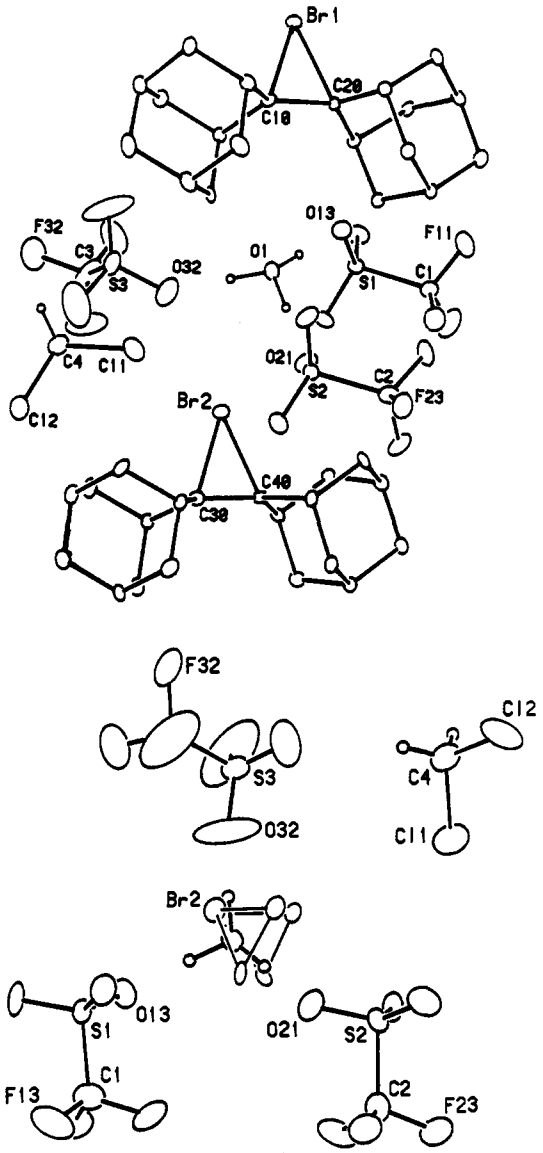


**Figure 1.** Two ORTEP views of the asymmetric unit in the structure of **1**-$Br^+OTf^-$. In Figure 1b (bottom) is a view of the asymmetric unit down the $Br_2$–$Br_1$ axis highlighting the $CF_3SO_3^-$, $H_3O^+$, and dichloromethane molecule. All carbon atoms of the adamantylidene groups except those bonded to $Br_1$ or $Br_2$ have been omitted for clarity.

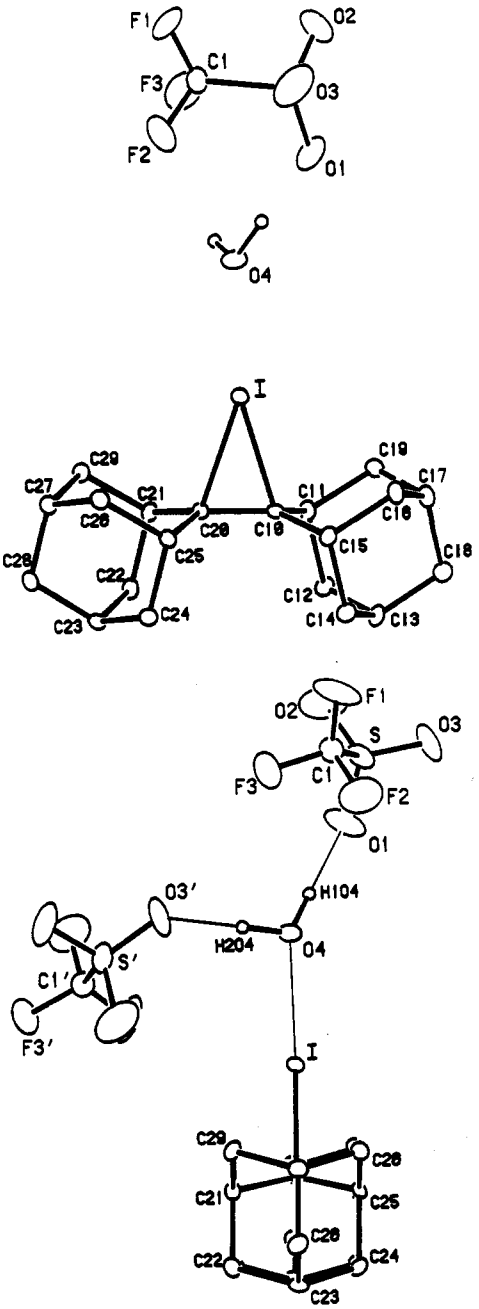


**Figure 2.** Two ORTEP views of the asymmetric unit of **1**-$I^+/OTf^-$. Figure 2b (bottom) shows an alternate view down the $C_{10}$–$C_{20}$ bond, illustrating the interaction of the water molecule with the iodonium ion and with symmetry-related triflate ions.

interactions between the $H_3O^+$ ion and each of the three $OTf^-$ ions result in formation of a layer separating the two independent bromonium ions. The source of the $H_3O^+$ is probably HOTf (itself the product of the reaction of $CH_3OTf$ with adventitious $H_2O$).

Given in Table 2a are selected bond lengths and angles for **1**-$Br^+/OTf^-$, which are compared with those previously determined[2b] for **1**-$Br^+/Br_3^-$. The selected data show that the two types of bromonium ions, one with $Br_3^-$ and the other two with $OTf^-$ as counterions, are essentially indistinguishable. The average C–C bond lengths for the adamantylidene groups are the same (1.534 Å for **1**-$Br^+/OTf^-$; 1.532 Å for **1**-$Br^+/Br_3^-$). The only notable differences occur in the three-membered rings containing the Br and two C atoms. For **1**-$Br^+/Br_3^-$ the bromine atom is displaced toward $C_{10}$ from a symmetrical position: the result is a Br–$C_{10}$ bond which is about 0.08 Å longer than the Br–$C_{10}$ bond in **1**-$Br^+/OTf^-$ and a Br–$C_{10}$–$C_{20}$ angle which is larger than the Br–$C_{20}$–$C_{10}$ angle. The pairs of Br–C bonds (Br–$C_{10}$ and Br–$C_{20}$, Br–$C_{30}$ and Br–$C_{40}$) in the two bromonium ions in **1**-$Br^+/OTf^-$ are nearly equivalent, which indicates that these ions are nearly symmetric species, as expected, and that the source of the bromonium ion asymmetry observed in **1**-$Br^+/Br_3^-$ is the placement of the $Br_3^-$.

The corresponding iodonium ion, **1**-$I^+/OTf^-$, crystallizes as a monohydrate (Figure 2a), the source of $H_2O$ being adventitious water or water introduced during the handling for crystallization. The oxygen of the $H_2O$ lies 2.630 Å from the $I^+$, lying roughly along a line connecting the I atom and the center of the $C_{10}$–$C_{20}$ bond of the iodonium ion. The oxygen of the $H_2O$ is 2.796 and 2.752 Å from the oxygen atoms of two separate triflates (one belonging to the same asymmetric unit as the indicated iodonium ion and the other belonging to symmetry-related triflate at $(1 - x, {}^1/_2 + y, {}^1/_2 - z)$. This is best visualized in the view down the $C_{10}$–$C_{20}$ bond shown in Figure 2b, which suggests that the triflate counterions form a chain that also involves hydrogen bonds to the bridging $H_2O$. As for the iodonium ion itself, it is essentially symmetric, as indicated by the similarity of the I–C bond lengths and the I–C–C bond angles. The major structural differences

**Table 2.** Selected Interatomic Distances and Angles for **1**-$Br^+$/OTf$^-$, **1**-$Br^+$/$Br_3^-$, and **1**-$I^+$/OTf$^-$ Determined from X-ray Diffraction and from *ab Initio* SCF Calculations[a]

(a) **1**-$Br^+$/$Br_3^-$ and **1**-$Br^+$/OTf$^-$

| | **1**-$Br^+$/$Br_3^-$ [b] | **1**-$Br^+$/OTf$^-$ [c] | calculated[d] |
|---|---|---|---|
| | (i) Interatomic Distances (Å) | | |
| $C_{10}$–$C_{20}$ | 1.497(8) | 1.492(15) | 1.491 |
| ($C_{30}$–$C_{40}$) | | 1.491(14) | |
| Br–$C_{10}$ | 2.116(6) | 2.118(10) | 2.158 |
| (Br–$C_{30}$) | | 2.089(10) | |
| Br–$C_{20}$ | 2.194(6) | 2.136(10) | 2.158 |
| (Br–$C_{40}$) | | 2.114(20) | |
| $O_1$–$O_{13}$ | | 2.55(2) | |
| $O_1$–$O_{21}$ | | 2.49(2) | |
| $O_1$–$O_{32}$ | | 2.50(2) | |
| | (ii) Interatomic Angles (deg) | | |
| C–$C_{10}$–C | 113.1(5) | 111.2(8) | 111.3 |
| (C–$C_{30}$–C) | | 112.1(5) | |
| C–$C_{20}$–C | 112.7(5) | 112.9(9) | 111.3 |
| (C–$C_{40}$–C) | | 112.7(5) | |
| $C_{10}$–Br–$C_{20}$ | 40.6(2) | 41.0(5) | 40.4 |
| ($C_{30}$–Br–$C_{40}$) | | 41.6(4) | |
| Br–$C_{10}$–$C_{20}$ | 72.5(3) | 70.1(6) | 69.8 |
| (Br–$C_{30}$–$C_{40}$) | | 70.2(6) | |
| Br–$C_{20}$–$C_{10}$ | 66.9(3) | 68.8(7) | 69.8 |
| (Br–$C_{40}$–$C_{30}$) | | 68.3(6) | |

(b) **1**-$I^+$/OTf$^-$

| | observed | calculated |
|---|---|---|
| | (i) Interatomic Distances (Å) | |
| $C_{10}$–$C_{20}$ | 1.454(6) | 1.485 |
| I–$C_{10}$ | 2.362(6) | 2.389 |
| I–$C_{20}$ | 2.338(6) | 2.389 |
| I–$O_4$ | 2.630(4) | |
| $O_4$–$O_1$ | 2.796(8) | |
| $O_4$–$O_3'$ | 2.752(8) | |
| | (ii) Interatomic Angles (deg) | |
| C–$C_{10}$–C | 110.6(5) | 110.9 |
| C–$C_{20}$–C | 111.8(5) | 110.9 |
| $C_{10}$–I–$C_{20}$ | 36.0(1) | 36.2 |
| I–$C_{10}$–$C_{20}$ | 71.1(4) | 71.9 |
| I–$C_{20}$–$C_{10}$ | 72.9(4) | 71.9 |

[a] Numbers in parentheses are estimated standard deviations in the least significant digits. For atom numbering, see Figure 1a,b and Figure 2a,b. [b] Reference 2b. Although the numbering scheme for **1**-$Br^+$/$Br_3^-$ is not identical to that for **1**-$Br^+$OTf$^-$, the analogous quantities are cited. [c] The two sets of data correspond to the two independent bromonium ions found in the unit cell of **1**-$Br^+$/OTf$^-$. [d] Calculated as described in section d.

between the iodonium and bromonium ions are the longer C–I bond (2.35 vs 2.11 Å for C–Br) and slightly shorter center $C_{10}$–$C_{20}$ bond (1.45 vs 1.49 Å). See Table 2 for a comparison of selected interatomic distances and angles in **1**-$I^+$/OTf$^-$ with the analogous quantities in **1**-$Br^+$/$Br_3^-$ and **1**-$Br^+$/OTf$^+$.

**(b) $^{13}C$ NMR and $X^+$ Site Exchange.** Given in Table 1 are $^{13}C$ chemical shifts for the various iodonium and bromonium ions of **1** and **2** in $CD_2Cl_2$. The numbering scheme is based on that shown in eq 3, which allows easy comparison with the assignments made by Olah et al.[2a] for **1**-$Br^+$ and **1**-$I^+$: the chemical shifts for **1** and **2** are also included in Table 1. Assignments were confirmed by APT experiments.

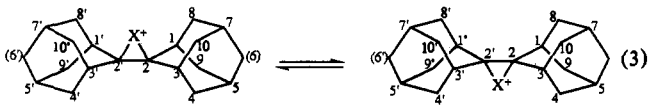

(3)

At low temperature (−80 °C) and in the absence of added olefin, a slow exchange condition is satisfied wherein the $^{13}C$ spectra provide evidence that ions **1**-$Br^+$/OTf$^-$, **2**-$Br^+$/OTf$^-$, **1**-$I^+$/OTf$^-$, and **2**-$I^+$/OTf$^-$ each possess two perpendicular planes of symmetry. One plane contains the $C_2$, $C_{2'}$, and X atoms of the halonium ion, and the other plane contains the X atom and bisects the $C_2$–$C_{2'}$ bond. The $^{13}C$ resonances for the carbons on the top side of the molecule ($C_{8,8',10,10'}$) adjacent to the $X^+$ in the left-hand structure of eq 3 are, in all cases, downfield from their counterparts ($C_{4,4',9,9'}$) on the bottom side. $C_{7,7'}$ and $C_{5,5'}$ are also distinct in all ions studied in this work except **2**-$Br^+$/OTf$^-$. Addition of a small amount of the parent olefin to a solution of a halonium ion causes the peaks for $C_{8,8',10,10'}$ and $C_{4,4',9,9'}$, and those for $C_{7,7'}$ and $C_{5,5'}$, to broaden, then coalesce, and ultimately give a single narrow line for $C_{4,4',8,8',9,9',10,10'}$, and one for $C_{5,5',7,7'}$ as more olefin is added. These observations indicate that the two-step exchange process translocates the $X^+$ from the top side of the halonium ion to the bottom side (eq 4). A detailed analysis

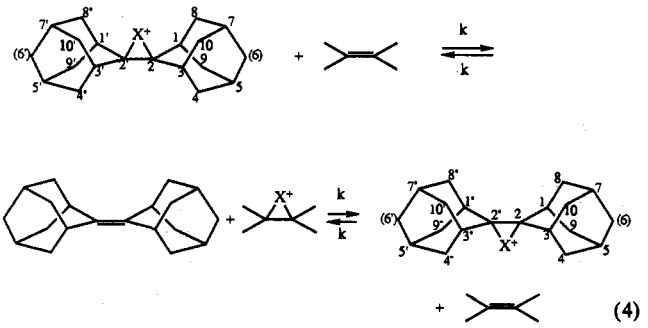

(4)

of this process shows that, since [added olefin] ≪ [halonium ion], the magnetizations of the olefin carbon nuclei do not contribute significantly to the spectrum, and that the transfer of magnetization between sites $C_{8,8',10,10'}$ and $C_{4,4',9,9'}$ is a pseudo-first-order process characterized by rate constant

$$k_{app} = k[\text{olefin}]/2$$

The fact that the rate of the transfer process depends upon [added olefin] requires that it must proceed via an olefin:ion complex and that a given halonium ion completely transfers its $X^+$ to the acceptor olefin prior to once again receiving the $X^+$ at either of the now equivalent sides of the π-bond. These experiments proved to be unfeasible for **2**-$Br^+$/OTf$^-$ since some decomposition was noted over the several hour period required for a detailed study of the exchange kinetics.

Analysis of the shapes of the NMR lines from the $C_{8,8',10,10'}$ and $C_{4,4',9,9'}$ carbons yielded the pseudo-first-order rate constants, $k_{app}$, for the site exchange. The values of $k_{app}$ at −80 °C for various concentrations of added olefin are given in Table 3S (supplementary material) and are plotted in Figures 3 and 4 for

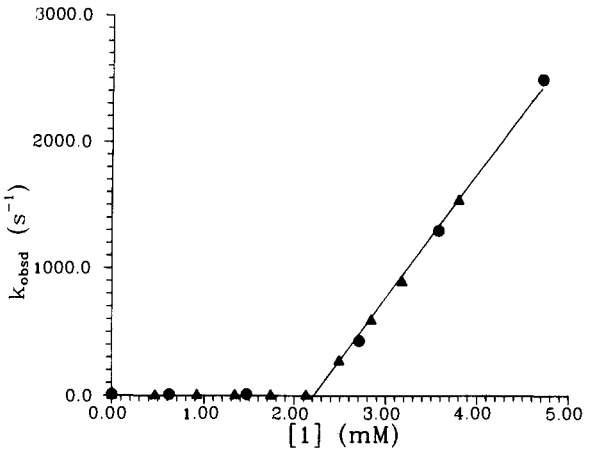


**Figure 3.** A plot of the first-order rate constants ($k_{app}$) for site exchange within **1**-$Br^+$/OTf$^-$ as a function of added [Ad=Ad]; $CD_2Cl_2$ solvent, −80.2 °C. Circles and triangles represent data from two independent NMR experiments each using half of a ~100 mM stock solution of **1**-$Br^+$/OTf$^-$.

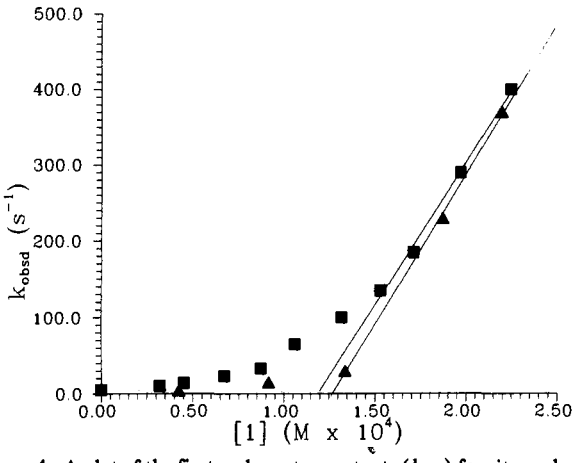


**Figure 4.** A plot of the first-order rate constants ($k_{app}$) for site exchange within **1**-$I^+$/$OTf^-$ as a function of added [Ad=Ad]; $CD_2Cl_2$ solvent, −79 ± 2 °C. Squares and triangles represent data from two independent NMR experiments.

**1**-$Br^+$/$OTf^-$ and **1**-$I^+$/$OTf^-$. A similar plot (not shown) is observed for **2**-$I^+$/$OTf^-$. The uncertainties in $k_{app}$ are ~10% in the intermediate ranges and may be as high as 20% near the slow and fast exchange limits.

The shapes of the plots of $k_{app}$ vs [added olefin] in Figures 3 and 4 warrant explanation since each reveals a break which indicates that the first additions of olefins cause very little site exchange, but that further additions, beyond the break point, cause large increases in the exchange rate. When first prepared and subjected to $^{13}C$ NMR analysis, only **1**-$Br^+$/$OTf^-$ was observed to be in the slow exchange limit at −80 °C. Solutions of ions **1**-$I^+$/$OTf^-$ and **2**-$I^+$/$OTf^-$, in our hands, could never be prepared in sufficiently pure states to exhibit slow exchange. The major impurities undoubtedly include unreacted olefin which, of course, facilitates the site exchange. By the manner of its preparation from Ad=Ad, $Br_2$, and $CH_3OTf$, **1**-$Br^+$/$OTf^-$ contains slight impurities of HOTf (clearly present in the crystal structure in Figure 2a,b), which we surmise is capable of protonating residual or added Ad=Ad, thereby preventing it from promoting the site exchange. Thus, the break in the plot in Figure 3 results from the titration of adventitious HOTf by the initial addition of olefin, followed by a linear increase in the exchange rate with free olefin concentration once all of the HOTf has reacted. The slope of the linear portion of $k_{app}$ vs [added Ad=Ad] is $k/2$, where $k$ is the second-order rate constant for transfer of $Br^+$ from **1**-$Br^+$ to Ad=Ad. At −80 °C, $k = 2.0 \times 10^6$ $M^{-1}$ $s^{-1}$.

In the exchange studies on **1**-$I^+$/$OTf^-$, a small amount of HOTf was added to the original solution in order to protonate any unreacted olefin present. The carbon NMR spectrum obtained after this addition was the anticipated one for a species with distinct top and bottom sides. The two plots in Figure 4 show once again that added olefin serves initially to titrate the excess HOTf, after which further additions of **1** promote the site exchange process involving the iodonium ion and free olefin. It should be noted that the accessible range of $k_{app}$ for the **1**-$I^+$/$OTf^-$ site exchange is 1 order of magnitude smaller than the ranges for the **1**-$Br^+$/$OTf^-$ and **2**-$I^+$/$OTf^-$ systems. The breaks in the $k_{app}$ vs [added **2**] curves are therefore less well-defined than the break in Figure 3, and the value of the rate constant, $k$, for the exchange of $I^+$ from **1**-$I^+$ to **1** is less precise ($(7.6 \pm 0.8) \times 10^6$ $M^{-1}$ $s^{-1}$ at −80 °C).

As described in the previous section, the addition of HOTf to a solution of **2**-$I^+$/$OTf^-$ did not suppress the exchange process. Instead, the solutions were treated with AgOTf to complex the residual olefin. Initial additions of **2** to this treated solution cause complexation of the excess $Ag^+$, while further additions lead to enhanced rates of site exchange. The rate constant, $k$, for the transfer of $I^+$ between **2**-$I^+$ and **2** is $(4.2 \pm 0.4) \times 10^6$ at −80 °C.

The observed similarity of the values of the rate constants for transfer of $X^+$ between the halonium ion and the parent hydrocarbons for the three systems studied and the high numerical values of the rate constants suggests that the rates of $X^+$ exchange may be dominated by the rates of encounter of halonium ion and olefin rather than by energetics. It was therefore of interest to determine the activation parameters for the $X^+$ exchange process between **1**-$Br^+$/$OTf^-$ and Ad=Ad (**1**). Small aliquots of a solution of **1** in $CD_2Cl_2$ were added to a solution containing ~100 mM **1**-$Br^+$/$OTf^-$ (both solutions maintained at ca. −80 °C) until the resonances for $C_{8,8',10,10'}$ and $C_{4,4',9,9'}$ broadened sufficiently that a reliable measurement of the exchange rates could be made by line-shape analysis. The $^{13}C$ spectrum was then obtained at six temperatures between −103 and −51 °C, and the rate constants for the site exchange were evaluated. Analysis of the data ($T$, $k_{obs}$ ($s^{-1}$); −103.1°, 200; −90.9°, 350; −80.6°, 450; −70.9°, 650; −60.3°, 800; −51.3°, 900) yielded the activation parameters $\Delta H^{\ddagger} = 1.8 \pm 0.2$ kcal $mol^{-1}$ and $\Delta S^{\ddagger} = -21 \pm 1$ cal $K^{-1}$ $mol^{-1}$.[7] The enthalpy of activation is essentially identical to the Arrhenius activation energy (1.7 kcal/mol) for viscous flow in methylene chloride.[8] It appears, therefore, that the exchange of $Br^+$ between **1**-$Br^+$ and **1**, and by inference the exchange of $I^+$ between an iodonium ion and olefin, is largely an entropy-driven process which is encounter-limited. The diffusion-controlled encounter rate of two spheres of radii $r_A$ and $r_B$ in a medium of viscosity $\eta$ at temperature $T$ is characterized by a rate constant[9]

$$k_{diff} = \frac{2RT(r_A + r_B)^2}{3000\eta r_A r_B}$$

If we assume $r_A \simeq r_B$ and we estimate the viscosity of $CD_2Cl_2$ to be 0.019 P at −80 °C by extrapolation of available viscosity data,[8] the value of $k_{diff}$ is $2.3 \times 10^9$ $M^{-1}$ $s^{-1}$. The large difference between $k_{diff}$ and the observed values of $k$ for the halonium/olefin exchange reactions is undoubtedly due to the stringent orientation requirement for reactive encounters.

**(c) Calculations on the Energy Profile of the Reaction $C_2H_4X^+ + C_2H_4 \rightleftharpoons C_2H_4 + C_2H_4X^+$, X = Br, I.** As a simple model for the halonium ion/olefin exchange reaction, we investigated the $X^+$ transfer between two ethylene moieties using *ab initio* calculations. The transfer of $X^+$ can be visualized by considering the approach, from above, of an ethylene molecule, with its C–C bond lying along the $x$-axis, toward a $C_2H_4X^+$ ion centered at the origin of coordinates with the X atom lying on the $z$-axis and the C–C bond along the $y$-axis. (Calculations showed that the conformation with the two C–C bonds parallel is of higher energy.) It is convenient to use $C_{2v}$ labeling of orbitals to describe the electronic changes which occur during the course of the reaction since the symmetry of the system is $C_{2v}$ except at the transition state, where it has $D_{2d}$ symmetry.

In order to minimize computational effort and reduce the possible impact of basis set superposition error, effective core potentials[10] were used for C, Br, and I. Two basis sets with compositions given in Table 3 were used in the calculations. Basis set A leads to fairly compact molecular basis sets for $C_2H_4$, $C_2H_4X^+$, and $(C_2H_4)_2X^+$ (48, 70, and 118 functions, respectively) suitable for MCSCF calculations. The static dipole polarizability component $\alpha_{zz}$ of ethylene calculated with this basis is too low,

(7) Error limits from standard deviations of the Eyring plot of $\ln(k/T)$ vs $1/T$, where $k$ (from line-shape analysis) is given a 15% uncertainty.

(8) Washington, E. W., Ed. *International Critical Tables of Numerical Data*; McGraw-Hill Book Co.: New York, 1930; Vol. VII, p 218.

(9) Jordan, R. B. *Reaction Mechanisms of Inorganic and Organometallic Systems*; Oxford University Press: New York, 1991; p 20.

(10) Stevens, W. J.; Basch, H.; Krauss, M. *J. Chem. Phys.* **1984**, *81*, 6026. Stevens, W. J.; Krauss, M.; Basch H.; Jasien, P. G. *Can. J. Chem.* **1992**, *70*, 612.

(11) Huzinaga, S. *J. Chem. Phys.* **1965**, *42*, 1293.

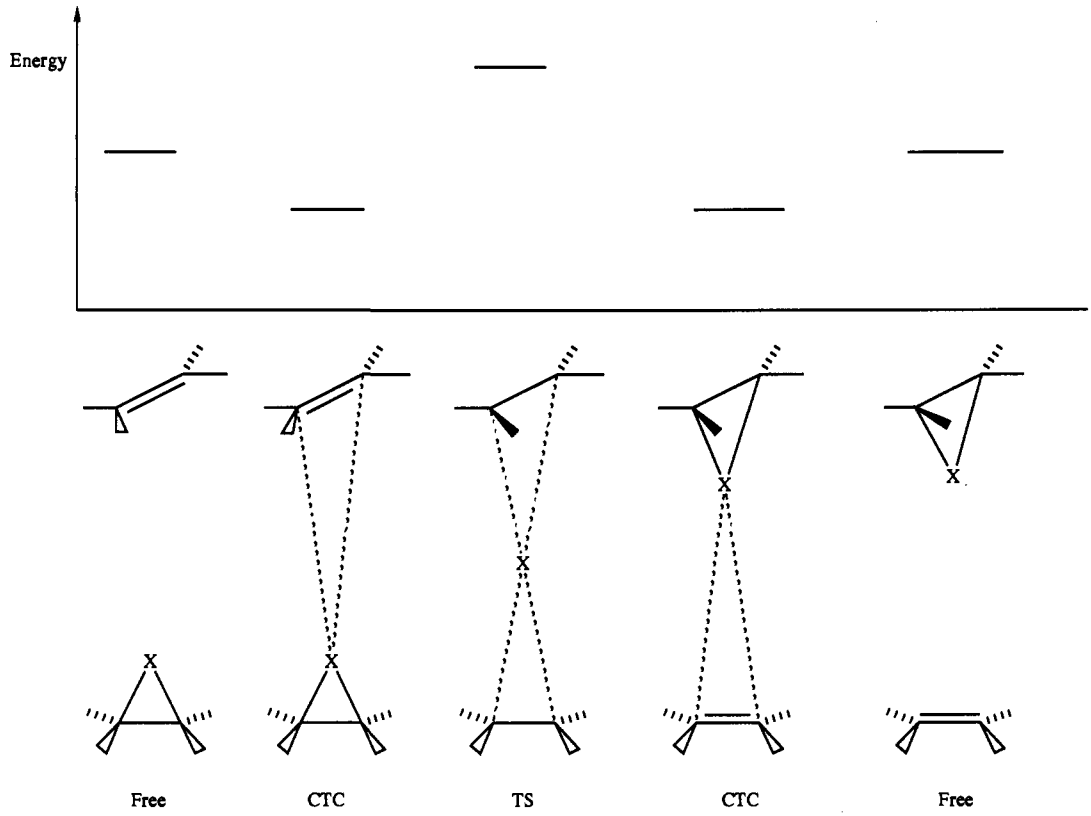


**Figure 5.** Schematic representation of the calculated energy changes that occur as the ethylene and halonium ions progress along the reaction path for $X^+$ transfer.

indicating that the basis may be too rigid and might give unreliable estimates of the interactions between $C_2H_4$ and $C_2H_4X^+$ and of the barrier to $X^+$ exchange. The basis was therefore extended by adding diffuse functions to the hydrogen and carbon basis sets,[12] and this second basis set (basis B) gives accurate dipole polarizability components for ethylene. In order to describe the changes in bonding which occur when $X^+$ is transferred from $C_2H_4X^+$ to $C_2H_4$ as accurately as possible, multiconfiguration self-consistent field (MCSCF) calculations were used. Unfortunately, the sizes of the molecular basis sets for $C_2H_4X^+$ and $(C_2H_4)_2X^+$ (106 and 190 functions, respectively) constructed with basis B were too large to permit calculations at the MCSCF level, and calculations with basis B were limited to the SCF level. The full orbital reaction space (FORS) wave functions[14] were used for the MCSCF calculations. A FORS wave function includes all possible distributions of the active electrons (those involved in bond formation and breaking) among the active molecular orbitals, subject to the constraint that space and spin symmetry be preserved. For this work, the wave function was designed to correlate electrons in the C–C and C–X bonds, and the active spaces for the systems are given in Table 4. For ethylene, the active space includes the $\pi$- and $\pi^*$-orbitals. For $C_2H_4X^+$, the space also contains the three-center MOs of $b_2$ and $a_1$ symmetry, which are involved in bonding in the C–X–C fragment, and the $b_1$ MO (the $p_x$-orbital on X), which is included to give a clear description of the changes in electron densities as the system passes from isolated $C_2H_4$ and $C_2H_4X^+$ entities through the $C_2H_4$–$C_2H_4X^+$ charge-transfer complex and on into the $[C_2H_4$–X–$C_2H_4]^+$ transition state. The number of configurational-state functions in the MCSCF wave functions were small enough (see

**Table 3.** Atomic Gaussian Basis Sets Used in the Calculations

| | basis A | | | basis B[a] | |
|---|---|---|---|---|---|
| atom | U[b] | C[c] | X[d] | C[c] | X[d] |
| H | (4s)[e] | (31) | $\zeta_p = 1.10$ | | $\zeta_s = 0.04$[f] $\zeta_p = 0.07$[f] |
| C | (4s4p)[g] | (31/31) | $\zeta_d = 0.80$ | (211/211) | $\zeta_d = 0.175$[f] |
| Br | (5s5p)[g] | (2111/2111) | $\zeta_d = 0.389$[h] | | |
| I | (5s5p)[g] | (2111/2111) | $\zeta_d = 0.266$[h] | | |

[a] Basis A is augmented as specified in column X to obtain basis B. [b] Uncontracted basis set composition. [c] Contracted basis set structure. [d] Additional functions. [e] From ref 11. [f] From ref 12. [g] From ref 10. [h] From ref 13.

**Table 4.** MCSCF FORS Wave Functions

| | | | | $C_0$[a] | |
|---|---|---|---|---|---|
| system | active space | no. CSF[b] | | Br | I |
| $C_2H_4$ | $a_1^2b_2^0$ | 2 | | 0.976 | 0.976 |
| $C_2H_4Br^+$ | $a_1^2b_2^2b_1^2\,a_1^0b_2^0$ | 18 | | 0.968 | 0.973 |
| $(C_2H_4)_2Br^+$ | $a_1^2b_2^2b_1^2a_1^2\,a_1^0b_2^0b_1^0$ | 142 | CTC: | 0.9055 | 0.944 |
| | | | TS: | 0.950 | 0.951 |

[a] $C_0$ is the coefficient of the Hartree–Fock configuration in the MCSCF/FORS wave function. [b] Number of terms (configurational-state functions) in the MCSCF expansion.

Table 4) to permit the use of efficient gradient techniques for geometry optimization (Gaussian 90 code[15] for the SCF calculations, and the GAMESS[16] and HONDO[17] for the MCSCF wave functions). The character of the SCF potential surface at the transition-state geometry was inspected using the Hessian matrix of the total energy, and the genuine nature of the transition

(12) Spackman, M. A. *J. Phys. Chem.* **1989**, *93*, 7594.
(13) Andzelm, J.; Huzinaga, S. (Ed.); Klobukowski, M.; Radzio-Andzelm, E.; Sakai, Y.; Tatewaki, H. *Gaussian Basis Sets For Molecular Calculations*; Elsevier: Amsterdam, 1984.
(14) Ruedenberg, K.; Sundberg, K. R. In *Quantum Science*; Calais, J. L., Goscinski, O., Linderberg, J., Ohrn, Y., Eds.; Plenum: New York, 1976; pp 505–515. Cheung, L. M.; Sundberg, K. R.; Ruedenberg, K. *Int. J. Quantum Chem.* **1976**, *16*, 1103.
(15) Frisch, M. J.; Head-Gordon, M.; Trucks, G. W.; Foresman, J. B.; Schlegel, H. B.; Raghavachari, K.; Robb, M. A.; Binkley, J. S.; Gonzalez, C.; DeFrees, D. J.; Fox, D. J.; Whiteside, R. A.; Seeger, R.; Melius, C. F.; Baker, J.; Martin, R. L.; Kahn, L. R.; Stewart, J. J. P.; Topiol, S.; Pople, J. A. *Gaussian 90*; Gaussian, Inc.: Pittsburgh, PA, 1990.
(16) Schmidt, M. W.; Baldridge, K. K.; Boatz, J. A.; Jensen, J. H.; Koseki, S.; Gordon, M. S.; Nguyen, K. A.; Windus, T. L.; Elbert, S. T. *QCPE Bull.* **1990**, *10*, 52.

**Table 5.** Optimized Geometrical Parameters[a]

| structure | parameter | X = Br MCSCF | X = I MCSCF |
|---|---|---|---|
| 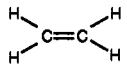 | C–C | 1.369 | |
| | C–H | 1.093 | |
| | H–C–H | 117.4 | |
| 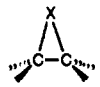 | C–C | 1.458 | 1.453 |
| | C–H | 1.089 | 1.089 |
| | C–X | 2.069 | 2.275 |
| | H–C–X | 108.0 | 107.6 |
| | H–C–H | 118.0 | 117.8 |
| | C–C–X | 69.4 | 71.4 |
| | (HHC)–C | 16.3 | 17.2 |
| 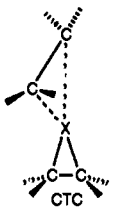 | C–C | 1.369 | 1.376 |
| | C–H | 1.093 | 1.093 |
| | H–C–H | 117.3 | 117.3 |
| | C–X | 3.432 | 3.517 |
| | H–C–X | 97.7 | 97.7 |
| | C–C–X | 78.5 | 78.8 |
| | (HHC)–C | 3.3 | 3.7 |
| CTC | C–C | 1.453 | 1.446 |
| | C–H | 1.089 | 1.089 |
| | C–X | 2.075 | 2.290 |
| | H–C–X | 107.9 | 107.3 |
| | H–C–H | 118.0 | 117.8 |
| | C–C–X | 69.5 | 71.6 |
| | (HHC)–C | 16.2 | 16.6 |
| | C–C | 1.392 | 1.391 |
| | C–H | 1.089 | 1.090 |
| | C–X | 2.459 | 2.636 |
| | H–C–X | 101.6 | 101.4 |
| | H–C–H | 117.9 | 117.8 |
| | C–C–X | 73.6 | 74.7 |
| TS | (HHC)–C | 6.4 | 7.2 |

[a] Calculated with basis A.

state was confirmed by the existence of a single negative eigenvalue. The mode-following search technique[18] was used to locate the transition state on the MCSCF surface. The optimized MCSCF values of the geometrical parameters for the various entities involved in the schematic reaction path illustrated in Figure 5 are given in Table 5.

Since there are only minor differences in the geometrical parameters calculated with MCSCF and SCF wave functions, the largest difference being in the C–C and C–X bond lengths, which are slightly longer in the MCSCF results, the SCF results are omitted for brevity. The magnitudes of the coefficients of the Hartree–Fock configurations in the MCSCF wave functions at the optimized MCSCF geometries (Table 4) indicate that the Hartree–Fock configuration (the SCF wave function) dominates the wave functions for the charge-transfer and transition-state complexes as well as those for the reactants. Comparison of the structures of the $C_2H_4$–$C_2H_4X^+$ charge-transfer complex with those of the isolated reactants, $C_2H_4$ and $C_2H_4X^+$, shows that there are only minor changes in the geometry of the ethylene molecule; in particular, the angle between the C–C bond and the HHC plane, denoted (HHC)–C in Table 5, is very close to 0, as in ethylene. In the transition state, the geometrical parameters are close to the averages of the values for the isolated systems. The distances between carbon and iodine are 0.18–0.24 Å longer than those between carbon and bromine, which is consistent with the 0.19-Å difference in the covalent radii of I and Br[19] and with the structural data of Table 2. It should be noted that the SCF results for the bromonium ion are similar to those obtained by Hamilton and Schaefer[20] using a DZ+d basis, which confirms the expected reliability of the effective core potentials used here.

(17) (a) Dupuis, M.; Watts, J. D.; Villar, H. O.; Hurst, G. J. B. *QCPE Bull.* **1988**, *8*, 79. (b) Dupuis, M.; Maluendes, S. A. In *Modern Techniques in Computational Chemistry: MOTECC-91*; Clementi, E., Ed.; ESCOM: Leiden, 1991; pp 469–534.
(18) Baker, J. *J. Comput. Chem.* **1986**, *7*, 385.
(19) Emsley, J. *The Elements*; Clarendon Press: Oxford, 1989.

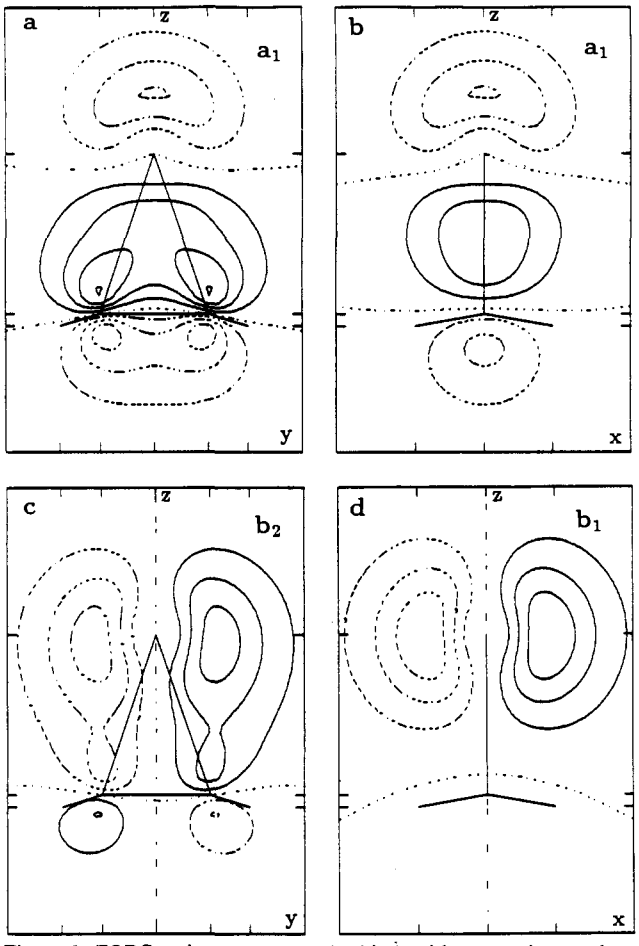


**Figure 6.** FORS active space natural orbitals with occupation numbers greater than 1 for $C_2H_4I^+$: (a) $a_1$ in *yz* plane, (b) $a_1$ in *xz* plane, (c) $b_2$ in *yz* plane, (d) $b_1$ in *xz* plane. The occupation numbers of the orbitals are 1.940 (1.950), 1.962 (1.969), and 1.998 (1.998) for $a_1$, $b_2$, and $b_1$ orbitals, respectively (the values for $C_2H_4Br^+$ are in parentheses).

The active orbitals for the reactant $C_2H_4I^+$, the $C_2H_4$–$C_2H_4I^+$ charge-transfer complex, and the $[C_2H_4\text{–I–}C_2H_4]^+$ transition state are shown in Figures 6–8. The analogous plots for the bromonium system are similar. The bonding in the free halonium ion, $C_2H_4X^+$, may be described as originating from the interaction between the empty $p_z$-orbital of the $X^+$ cation with the $\pi$-orbital of ethylene ($a_1$ MO, Figure 6a,b), accompanied by the back-donation of the electronic charge from the occupied $p_y$-orbital into the ethylene $\pi^*$-orbital ($b_2$ MO, Figure 6c). The net result is that the positive charge of +1 on the X atom in the free cation is substantially reduced in the halonium ion. The Mulliken atomic charges are +0.14 and +0.26 on Br and I atoms, and the corresponding Löwdin populations are +0.35 and +0.49. Bearing in mind that these population analyses provide only a broad picture of the charge distribution, it is useful to investigate the nature of the bonding in $C_2H_4I^+$ by examining the Mulliken population analyses of the $a_1$, $b_2$, and $b_1$ MCSCF MOs (Figure 6). These populations give a picture of the bonding in $C_2H_4I^+$, in which 1.06 electrons are donated to I from the ethylene $\pi$-orbital and 0.40 electrons are back-donated from I to ethylene, giving a net donation of 0.66 electrons from ethylene to iodine. Further electron transfer from ethylene to iodine occurs via the remaining doubly occupied orbitals which are not in the active space, bringing the overall charge on iodine to +0.26. The bonding here qualitatively resembles that in the $C_2H_4$–$Ag^+$ complex,[21] but the metal orbitals involved are different: the $\sigma$-donation in the halonium systems

(20) Hamilton, T. P.; Schaefer, H. F., III. *J. Am. Chem. Soc.* **1990**, *112*, 8260.
(21) Basch, H. *J. Chem. Phys.* **1972**, *56*, 441. Ziegler, T.; Rauk, A. *Inorg. Chem.* **1979**, *18*, 1558.

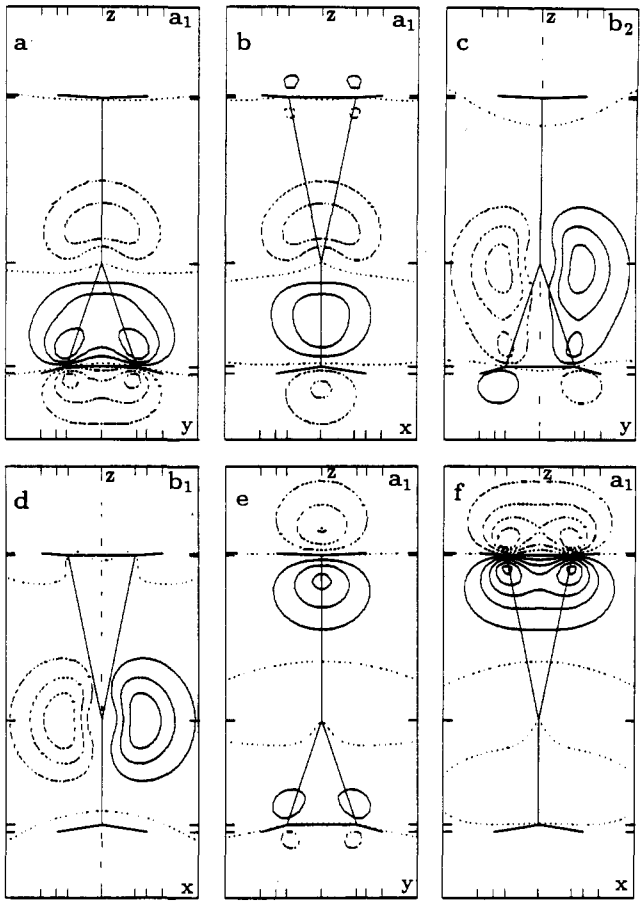


**Figure 7.** FORS active space natural orbitals with occupation numbers greater than 1 for the CTC $(C_2H_4IC_2H_4)^+$ ($C_{2v}$ symmetry): (a) $a_1$ in *yz* plane, (b) $a_1$ in *xz* plane, (c) $b_2$ in *yz* plane, (d) $b_1$ in *xz* plane, (e) $a_1$ in *yz* plane, (f) $a_1$ in *xz* plane. The occupation numbers are 1.940 (1.949), 1.963 (1.968), 1.998 (1.998), and 1.909 (1.909) for $a_1$, $b_2$, $b_1$, and $a_1$ orbitals, respectively (the values for $(C_2H_4BrC_2H_4)^+$ are in parentheses).

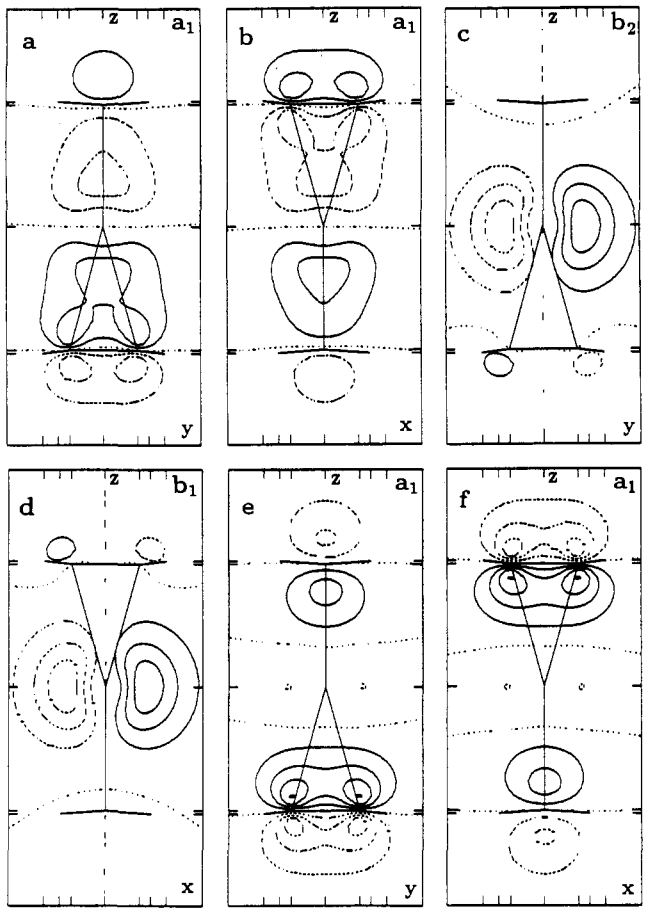


**Figure 8.** FORS active space natural orbitals with occupation numbers greater than 1 for the transition state $(C_2H_4IC_2H_4)^+$ ($D_{2d}$ symmetry): (a) $a_1$ in *yz* plane, (b) $a_1$ in *xz* plane, (c) $b_2$ in *yz* plane, (d) $b_1$ in *xz* plane, (e) $a_1$ in *yz* plane, (f) $a_1$ in *xz* plane. The occupation numbers are 1.946 (1.948), 1.986 (1.986), 1.986 (1.986), and 1.896 (1.892) for $a_1$, $b_2$, $b_1$, and $a_1$ orbitals, respectively (the values for $(C_2H_4BrC_2H_4)^+$ are in parentheses).

involves the X $p_z$-orbital in contrast to the Ag 5s orbital, and the X $p_y$-orbital rather than the Ag 4d orbital participates in $\pi$-back-bonding. The bonding in the $C_2H_4$–$C_2H_4X^+$ charge-transfer complex can be described in the same terms as in the halonium ion because the interaction between the halonium ion and the incoming ethylene molecule is small in the charge-transfer complex. As shown in Figure 7a-d, the $a_1$, $b_2$, and $b_1$ MOs strongly resemble the corresponding orbitals in the halonium ion, and the $a_1$ $\pi$-orbital of the adduct ethylene unit (Figure 7e,f) resembles that of the isolated ethylene molecule.

As the ethylene molecule approaches the halonium ion more closely than in the charge-transfer complex, the interaction between the doubly occupied $\pi$-orbital of ethylene and the partially occupied $p_z$-orbital on the X atom results in the formation of a five-center bonding $a_1$ MO (Figure 8a,b). At the same time, the lengthening of the C–X distance in the halonium moiety reduces the interaction between the occupied $p_y$-orbital on X and the $\pi^*$ MO on the ethylene fragment so that the $b_2$ MO is predominantly a $p_y$-orbital on X. As a result, the C–C bond length in the halonium ion decreases as the reacting species move toward the transition state. The filled $b_1$ MO of $C_2H_4X^+$ (essentially the $p_x$-orbital on X) donates electron density to the empty $\pi^*$-orbital of the incoming ethylene molecule, which results in an increased C–C distance in the ethylene. As the transition state is approached, the $b_1$ and $b_2$ orbitals become degenerate (see Figure 8c,d).

The calculated energy changes which occur as the ethylene and halonium ions progress along the schematic reaction path to the transition state shown in Figure 5 are given in Table 6. The charge-transfer complexes are more stable than the isolated reactants by 5–6 kcal/mol. The main difference between the bromonium and iodonium systems is in the energy difference between the transition state and the isolated reactants. The calculated activation energies for the bromonium system relative to the free reactants (and CTC) are 9.4 (4.6) kcal/mol at the SCF level and 13.5 (9.3) kcal/mol at the MSCF level, while those for the iodonium system are considerably smaller: between –4.6 (+1.6) kcal/mol (SCF) and 1.9 (6.6) kcal/mol (MCSCF). For the bromonium system, the energy barrier was also evaluated using SCF wave functions constructed with basis B in order to assess the effect of basis size on the computed activation energy, and the effects were found to be small. Zero-point energy corrections were evaluated for the bromonium system at the SCF level with basis A and were found to have similar values for reactant, charge-transfer complex, and transition-state species.

The computational approach used here provides clear insight into the nature of bonding in the halonium ions, the charge-transfer complexes, and the transition-state structures involved in the transfer of the halogen cation between two ethylene molecules, but it ignores the interactions between the halonium ion and its counterion and solute–solvent interactions. The calculated activation energies are appropriate only to the exchange reactions in the gas phase and differ from the values obtained from experimental measurements in solution.

**(d) Calculation of the Structure of Adamantylideneadamantane Bromonium Ion and Iodonium Ions.** The geometries of the two ions, **1-Br**$^+$ and **1-I**$^+$, were optimized using the gradient techniques incorporated in the GAMESS code.[16] Basis set A was used, leading to a total of 442 contracted molecular basis functions.

**Table 6.** Total Energies (in au) and Energy Differences[a] (in kcal mol$^{-1}$)

| structure | energy[b] | X = Br SCF | X = Br MCSCF | X = I SCF | X = I MCSCF |
|---|---|---|---|---|---|
| $C_2H_4$ | $E_T$(A) | −13.263 47 | −13.292 06 | −13.263 47 | −13.292 06 |
| | $E_T$(B) | −13.283 47 | | −13.283 47 | |
| $C_2H_4X^+$ | $E_T$(A) | −26.129 45 | −26.169 96 | −24.209 04 | −24.248 56 |
| | $E_T$(B) | −26.140 35 | | −24.221 63 | |
| $(C_2H_4XC_2H_4)^+$ | $E_T$(A) | −39.400 58 | −39.468 73 | −37.482 39 | −37.548 14 |
| CTC | $\Delta E$(A) | −4.8 | −4.2 | −6.2 | −4.7 |
| | $E_T$(B) | −39.430 71 | | −37.515 73 | |
| | $\Delta E$(B) | −4.3 | | −6.7 | |
| $(C_2H_4XC_2H_4)^+$ | $E_T$(A) | −39.385 58 | −39.447 27 | −37.479 78 | −37.537 64 |
| TS | $\Delta E$(A) | 4.6 | 9.3 | −4.6 | 1.9 |
| | $E_T$(B) | −39.417 91 | | −37.514 24 | |
| | $\Delta E$(B) | 3.7 | | −5.7 | |

[a] Energy differences are defined as $\Delta E = E_T[(C_2H_4XC_2H_4)^+] - [E_T(C_2H_4) + E_T(C_2H_4X^+)]$. [b] The letter in parentheses denotes the basis set used.

The optimized geometric parameters are collected in Table 2. The computed structural parameters of the free **1**-X$^+$ ions agree well with those in the X-ray structure of **1**-X$^+$/OTf$^-$. The calculated X–C$_{10}$ and C$_{10}$–C$_{20}$ bond lengths are longer than the experimental ones, indicating that a more flexible polarization space in the calculations might give improved bond lengths.

The calculated and observed C$_{10}$–C$_{20}$, X–C$_{10}$, and X–C$_{20}$ bond lengths in the **1**-X$^+$ ions are longer than the corresponding calculated C–C and C–X bond lengths in the $C_2H_4X^+$ ion, which undoubtedly reflect the steric effects produced by the bulky adamantane units in **1**-X$^+$.

**Supplementary Material Available:** Full X-ray structure reports including experimental details and tables of atomic coordinates, interatomic distances and angles, torsional angles, anisotropic thermal parameters (Tables 1S and 2S) and site exchange rate constants ($k_{obsd}$) for transfer of X$^+$ to added olefin as determined by $^{13}$C NMR line-shape analysis (Table 3S) (47 pages); tables of observed and calculated structure factors for **1**-Br$^+$/OTf and **1**-I$^+$/OTf (50 pages). This material is contained in many libraries on microfiche, immediately follows this article in the microfilm version of the journal, and can be ordered from the ACS; see any current masthead page for ordering information.